

Electron Dynamics in $\text{Nd}_{1.85}\text{Ce}_{1.15}\text{CuO}_{4+\delta}$: Evidence for the Pseudogap State and Unconventional c-axis Response

E.J. Singley, D.N. Basov

Department of Physics University of California San Diego, La Jolla, CA 92093-0319

K. Kurahashi*, T. Uefuji, K. Yamada

Institute for Chemical Research, Kyoto University, Uji 611-0011, Japan

Infrared reflectance measurements were made with light polarized along the a- and c-axis of both superconducting and antiferromagnetic phases of electron doped $\text{Nd}_{1.85}\text{Ce}_{1.15}\text{CuO}_{4+\delta}$. The results are compared to characteristic features of the electromagnetic response in hole doped cuprates. Within the CuO_2 planes the frequency dependent scattering rate, $1/\tau(\omega)$, is depressed below $\sim 650 \text{ cm}^{-1}$; this behavior is a hallmark of the pseudogap state. While in several hole doped compounds the energy scales associated with the pseudogap and superconducting states are quite close, we are able to show that in $\text{Nd}_{1.85}\text{Ce}_{1.15}\text{CuO}_{4+\delta}$ the two scales differ by more than one order of magnitude. Another feature of the in-plane charge response is a peak in the real part of the conductivity, $\sigma_1(\omega)$, at $50\text{-}110 \text{ cm}^{-1}$ which is in sharp contrast with the Drude-like response where $\sigma_1(\omega)$ is centered at $\omega = 0$. This latter effect is similar to what is found in disordered hole doped cuprates and is discussed in the context of carrier localization. Examination of the c-axis conductivity gives evidence for an anomalously broad frequency range from which the interlayer superfluid is accumulated. Compelling evidence for the pseudogap state as well as other characteristics of the charge dynamics in $\text{Nd}_{1.85}\text{Ce}_{1.15}\text{CuO}_{4+\delta}$ signal global similarities of the cuprate phase diagram with respect to electron and hole doping.

I. INTRODUCTION

The family of high temperature superconductors $\text{A}_{2-x}\text{Ce}_x\text{CuO}_4$, where A is a rare earth ion (Nd, Pr, Sm, Eu), has historically been considered an exception among copper oxides. Like all cuprates the basic building blocks of the structure are the CuO_2 layers. An important difference is that in the superconducting phases of $\text{A}_{2-x}\text{Ce}_x\text{CuO}_4$ lack the apical oxygen above the in-plane copper atom found in most hole doped cuprates. The charge carriers in $\text{A}_{2-x}\text{Ce}_x\text{CuO}_4$ are electrons rather than holes as in all other cuprate families.^{1,2} These materials have a relatively low T_c and early microwave measurements suggested the order parameter was *s*-wave³ in contrast with the *d*-wave symmetry established for hole doped compounds. However, more recent microwave measurements^{4,5}, along with photoemission⁶, and phase sensitive experiments⁷ indicate that the order parameter in $\text{Nd}_{1.85}\text{Ce}_{1.15}\text{CuO}_{4+\delta}$ (NCCO) and $\text{Pr}_{1.85}\text{Ce}_{1.15}\text{CuO}_{4+\delta}$ may in fact be *d*-wave. The most comprehensive infrared work on superconducting NCCO by Homes et al.⁸ found weak electron-phonon coupling below T_c , suggesting that NCCO, like other cuprates, is not a phonon-mediated superconductor. However, in contrast to other cuprates the in-plane superfluid was found to be anomalously large for a low T_c material, causing NCCO to deviate significantly from universal Uemera plot⁹. These results leave the nature of the relation between electron and hole doped cuprates ambiguous.

Previous doping dependent infrared studies have found that the evolution of spectral weight from the insulating parent compounds through the superconducting phases

is similar in both electron and hole doped cuprates.¹⁰⁻¹² Doping first moves spectral weight from above the charge transfer gap to the mid-infrared, and then to the Drude peak at $\omega = 0$. This implies that whether doped with electrons or holes the Mott-Hubbard insulator shows the same gross features in the electronic conductivity. Detailed studies on a variety of hole doped cuprates reveal a partial gap (pseudogap) in the spectrum of the low energy excitations.¹³ The pseudogap state is recognized as one of the key characteristics of the (hole doped) cuprates and is believed to be intimately connected to the origin of high- T_c superconductivity.¹⁴ So far, there have been no reports for a similar pseudogap region on the electron doped side of the phase diagram.¹⁵ With this in mind it is critical to determine whether there are principal differences in the fundamental interactions defining carrier dynamics and superconductivity in electron and hole doped Mott-Hubbard insulators. In short the question "Is NCCO a high temperature superconductor?"¹⁷ needs to be re-visited.

In this work we have determined the optical constants of $\text{Nd}_{1.85}\text{Ce}_{1.15}\text{CuO}_{4+\delta}$ for both the as grown antiferromagnetic (AF) phase and oxygen reduced superconducting (SC) samples. Special attention is paid to the low energy ($\omega < 100 \text{ meV}$) physics. Through an analysis of the in-plane scattering rate, $1/\tau(\omega)$, we find compelling evidence for a pseudogap in the electron doped materials. The doping and temperature dependence of the pseudogap is shown to mirror the behavior found in hole doped cuprates. Another important result is concerned with the non-monotonic behavior of $\sigma_1(\omega)$ in the far-infrared which is similar to that of disordered hole doped cuprates

and suggests charge carrier localization. We have also examined the interlayer *c*-axis conductivity of NCCO. A sum rule analysis demonstrates that nearly all of the interlayer superfluid is accumulated from an energy scale in excess of 8Δ , where Δ is the superconducting gap.

This paper is organized in the following manner. Section II gives a brief overview of the experimental procedures. The raw $R(\omega)$ data and the Kramers-Kronig generated $\sigma_1(\omega)$ for both the *a*- and *c*-axis of the SC and AF samples are presented in Section III. Section IV follows with a discussion of the key results. In sub-section IV-A we establish the existence of a pseudogap through the analysis of the in-plane scattering rate and discuss the implications of this result. Next, evidence for localization in the cuprates is presented in sub-section IV-B, and we elaborate on the impact of localization on both the DC and AC transport properties. Finally, sub-section IV-C discusses the energy scale related to the interlayer superfluid response. We conclude by summarizing our results in section V.

II. EXPERIMENTAL PROCEDURE

Single crystals of NCCO were prepared by the traveling-solvent-floating-zone method.¹⁸ The as-grown crystals are not superconducting, but show antiferromagnetic order with $T_N = 125$ K - 160 K.¹⁹ Superconductivity is achieved by deoxygenating the crystals. This process removes a small amount of apical oxygen atoms which are absent in the ideal T' structure.²⁰

The near normal reflectance was measured in polarized light from the far-infrared (FIR) to the near-ultraviolet. A Fourier transform spectrometer was used from 10 cm^{-1} to $18,000$ cm^{-1} , and a grating monochromator was used from $12,000$ cm^{-1} to $48,000$ cm^{-1} . After the reflectance was measured at various temperatures, the sample was coated in-situ with gold or aluminum and the measurements were repeated at all temperatures, providing an absolute measure of the reflectivity.²¹ The error in the absolute value of the reflectance is below 1%. The relative error in the reflectance measured at different temperatures does not exceed 0.1%.

To obtain the complex optical constants the Kramers-Kronig relations were used. In order to extend the reflectance data to higher energies the reflectance of $\text{Pr}_{1.85}\text{Ce}_{0.15}\text{CuO}_4$ from 6 eV to 38 eV was adopted.²² Above 38 eV the functional form $R \propto \omega^{-4}$ was assumed. When extrapolating the reflectance to zero frequency a Hagen-Rubens model was applied in the normal state, and a two-fluid model in the superconducting state. The error in the reflectance has been propagated to the optical constants and combined with uncertainties introduced by the extrapolation procedure, and will be discussed in the text.

III. REFLECTIVITY MEASUREMENTS AND KRAMERS-KRONIG ANALYSIS

A. *a*-axis

Fig. 1 shows the *a*-axis reflectance of the SC (Panel A) and AF (Panel B) samples in the FIR. The 292 K spectrum of the SC sample shows metallic behavior with a single phonon at 300 cm^{-1} . There is additional weak structure between 400 cm^{-1} and 700 cm^{-1} which grows in intensity as the sample is cooled. The reflectance of the SC sample shows a strong temperature dependence in the FIR. By 25 K the reflectance is nearly 5% above that at room temperature. Between 150 cm^{-1} and 300 cm^{-1} the reflectance of the SC sample at 25 K rivals that of such excellent conductors as Cu, Al, and Au yet the DC transport measurements indicate that the sample is a rather poor conductor.²³⁻²⁵ The resolution of this ambiguity can be found in the reflectance data below 150 cm^{-1} . Instead of $R(\omega)$ approaching 1 monotonically as $\omega \rightarrow 0$ as in a metal, the reflectance decreases giving rise to a peak in $R(\omega)$. As will be demonstrated later, this is a consequence of having poor conductivity at $\omega=0$ which greatly increases at finite frequencies. One final peculiarity of the SC sample is the lack of temperature dependence below T_c . The superconducting (7 K) reflectance increased slightly below 100 cm^{-1} , but at all higher frequencies the spectra was identical to the data at T_c (25 K) within 0.1%. The fact that the sample is truly a bulk superconductor can be confirmed by Fig. 4 where the *c*-axis reflectance changes dramatically below T_c .

The FIR reflectance of the AF sample (Panel B) is qualitatively different from its SC counterpart. The reflectance is lower at all temperatures and drops more quickly with increasing frequency. Notice that the *y*-axis of the top panel covers only 8% while the bottom panel extends from 85% - 100%. The phonon mode seen at 300 cm^{-1} is still clearly visible here. Three other modes that have been previously reported¹⁶ can also be identified at 130, 340, and 510 cm^{-1} . In addition a broad "hump" structure extending from 250 - 450 cm^{-1} is observed which grows in intensity as the temperature is lowered. No downturn in $R(\omega \rightarrow 0)$ is observed and at low temperatures $R(\omega < 300$ $\text{cm}^{-1})$ is nearly independent of frequency.

The right panel of Fig. 1 (C) shows the *a*-axis reflectance over an extended frequency range for both the SC and AF samples at 292 K and 25 K. The dominant feature of $R(\omega)$ in both samples is a plasma minimum at $\omega \sim 11,000$ cm^{-1} . The reflectance of the SC sample is $\sim 10\%$ higher than that of the AF sample in the mid-infrared, but drops below it near the plasma minima. In the SC sample $R(\omega)$ at 25 K smoothly joins the room temperature reflectance before the plasma minimum. In contrast to this behavior, in the AF sample the 25 K $R(\omega)$ curve crosses the 292 K spectrum at $1,000$ cm^{-1}

and in the low temperature spectrum reveals a partial gap-like depression at $\omega < 4,000 \text{ cm}^{-1}$. This structure has previously been reported by Onose and coworkers.¹⁶

Fig. 2 shows the real part of the conductivity, $\sigma_1(\omega)$, for the a-axis of the SC sample generated from the $R(\omega)$ data in Fig. 1. The most prominent feature is the peak in $\sigma_1(\omega)$ below 100 cm^{-1} . This should be contrasted with the behavior of conventional metallic systems which can be described by the Drude model:

$$\sigma_1^D(\omega) = \frac{\omega_p^2 \tau}{1 + \omega^2 \tau^2}. \quad (1)$$

where τ is the charge carrier lifetime, and ω_p is the plasma frequency which is determined by the ratio of the carrier density to effective mass. This form of the conductivity is a Lorentzian centered at $\omega = 0$. The peak in $\sigma_1(\omega)$ at $\omega \neq 0$ observed in NCCO signals a departure from conventional metallic transport. This is also evident from the non-monotonic behavior of $R(\omega)$ displayed in the top panel of Fig. 1. The peak in $\sigma_1(\omega)$ grows in strength and softens as the temperature is lowered. In the superconducting state the peak frequency shifts to 55 cm^{-1} and peak height is slightly reduced. The inset of Fig. 2 shows the 292 K and 25 K spectra, where the y-axis is nearly an order of magnitude smaller than in the main figure, and the scale of the x-axis extends up to $4,000 \text{ cm}^{-1}$ ($\simeq .5 \text{ eV}$). It is clear that the peak is a robust feature seen even at room temperature. Also notice that the 25 K curve is non-monotonic above the peak, showing a local minimum at 400 cm^{-1} . At higher frequencies $\sigma_1(\omega)$ decays slower than expected from Eq. 1.

In Fig. 3 $\sigma_1(\omega)$ is shown for the AF sample. The spectrum of $\sigma_1(\omega)$ at 292 K is flat and featureless. At 25 K a broad resonance is observed at $50 \text{ cm}^{-1} < \omega < 300 \text{ cm}^{-1}$. The AF sample has a semiconducting resistivity, so as $\omega \rightarrow 0$ the 25 K curve is expected to drop below the 292 K spectrum. As in the SC sample a minimum can be seen near 400 cm^{-1} at 25 K. The inset shows $\sigma_1(\omega)$ over an extended energy region for several different temperatures. At low temperatures an additional channel of absorption develops giving rise to a maximum at $\omega \simeq 2,200 \text{ cm}^{-1}$.¹⁶

B. c-axis

The c-axis reflectance for both the SC (solid lines) and AF (dashed-dotted line) samples is shown in Fig. 4. The two samples are very similar over most of the frequency range. The FIR reflectance is dominated by three strong phonon modes at 134 cm^{-1} , 268 cm^{-1} , and 507 cm^{-1} (right panel). At higher energies a flat featureless reflectance is observed up to $40,000 \text{ cm}^{-1}$ ($\sim 5 \text{ eV}$), after which the reflectance begins to rise. Both samples showed some temperature dependence in the phonon region. Above 700 cm^{-1} the reflectance of both samples was independent of temperature. Also note that at $\omega >$

60 cm^{-1} the reflectivity of the SC sample is the same above and below T_c . The left panel shows the detailed temperature dependence of the SC sample in the low energy region. At $T = T_c$ the reflectance is nearly flat with just a slight upturn as $\omega \rightarrow 0$. As the sample becomes superconducting a plasma minimum develops due to the screening by the superconducting current. This minimum deepens and moves to higher frequencies as the temperature is reduced.

Some of the key parameters defining the c-axis electro-dynamics of the normal and superconducting state can be determined directly from the raw $R(\omega)$ data. For this purpose we show the low frequency $R(\omega)$ data for the SC sample at 7 K and 25 K in the left panel of Fig. 5. The location of the minimum in $R(\omega)$ is the screened plasma frequency, ω_p^* . The screened plasma frequency quantifies the superfluid density, ρ_s , $\omega_p^* = \sqrt{\rho_s/\epsilon_\infty}$, where $\rho_s \propto n_s/m^*$ and n_s is the density of paired electrons and m^* is their effective mass. The reflectance can be expressed in terms of the dielectric function as: $R(\omega) = (\frac{\sqrt{\epsilon-1}}{\sqrt{\epsilon+1}})^2$. By letting $\epsilon = \text{constant}$, we can account for the nearly flat reflectance at T_c and just above the plasma minimum at lower temperatures below the frequency of the first phonon. Specifically a value of $\epsilon = 17$, gives a constant reflectance of 37% (dashed line). With this value of ϵ and the location of the minimum in $R(\omega)$ we determine $\rho_s = 3600 \text{ cm}^{-2}$ which corresponds to a c-axis penetration depth of $\lambda_c = c/\sqrt{\rho_s} = 26 \text{ }\mu\text{m}$. This value is confirmed by an analysis of the dielectric function generated from a Kramers-Kronig transformation of $R(\omega)$. Along these same lines we can gain an estimate for the DC conductivity at T_c directly from $R(\omega)$. We model the upturn seen in the reflectance of the 25 K spectrum as $\omega \rightarrow 0$ with ϵ and Eq. 1. A reasonable assumption for the spectra seen in Fig. 5 is $1/\tau \gg 100 \text{ cm}^{-1}$, therefore there is only one free parameter, $\omega_p^2 \tau = \sigma_{DC}$, and we obtain an excellent fit to the data with $\sigma_{DC} = 1.5 \text{ }\Omega^{-1}\text{cm}^{-1}$ (dotted line).

The right panel of Fig. 5 shows $\sigma_1(\omega)$ obtained from Kramers-Kronig transformation of $R(\omega)$ for the SC sample. The frequency range is confined to the region below the first phonon mode ($\omega < 120 \text{ cm}^{-1}$). The electronic contribution to the conductivity is extremely weak. For example, $\sigma_1(\omega = 10 \text{ cm}^{-1}) = 1.5 \text{ }\Omega^{-1}\text{cm}^{-1}$ at 25 K, which is the same value as was obtained from the fit of $R(\omega)$ in the left panel. Below T_c the temperature dependence of the low frequency conductivity is anomalous; at 10 cm^{-1} $\sigma_1(T_c) > \sigma_1(T = 7 \text{ K})$, however by 50 cm^{-1} $\sigma_1(T_c)$ has dropped below the conductivity at 7 K. Also notice that $\sigma_1(T = 19 \text{ K})$ is *greater than* $\sigma_1(T_c)$ throughout the entire frequency range depicted in Fig. 5.

An example of the error in $\sigma_1(\omega)$ is shown at 95 cm^{-1} for the $T = 25 \text{ K}$ spectrum. The error was calculated by propagating the uncertainty in the reflectance, and taking into account variations caused by different extrapolations of the reflectance to high and low frequencies. For the present analysis it is important to distinguish between absolute and relative errors. The absolute error

is shown by the large bars to be $\pm 1 \text{ } \Omega^{-1}\text{cm}^{-1}$. The relative error in the temperature dependence is an order of magnitude smaller and shown by the small bars.

IV. DISCUSSION

A. Electron dynamics in the CuO_2 plane: Pseudogap

A unique characteristic of the electron doped cuprates is the manner in which superconductivity is induced in the phase diagram. The as-grown crystals of $\text{Nd}_{2-x}\text{Ce}_x\text{CuO}_{4+\delta}$ progresses from an insulator at $x=0$ to a metal at $x=.21$ without the appearance of a superconducting phase. The superconducting state can only be realized by annealing the as-grown crystals in an oxygen free atmosphere.²⁶ While this procedure reduces the oxygen content by only $\simeq 1\%$ ²⁷ the changes in $\sigma_1(\omega)$ through out the infrared are significant. What can be drawn from Fig. 2 and Fig. 3 is that the AF sample is under doped with respect to the SC sample. To quantitatively compare the differences in $\sigma_1(\omega)$ Fig. 6 shows $\sigma_1^{SC}(\omega) - \sigma_1^{AF}(\omega)$ below $14,000 \text{ cm}^{-1}$. In the SC sample the mid-infrared absorption is reduced, while the low frequency ($\omega < 1,300 \text{ cm}^{-1}$) absorption increases. The inset shows the effective spectral weight, $N_{eff}(\omega) = \int_0^\omega \sigma_1(\omega')d\omega'$, for both the SC and AF sample. While the low energy spectral weight grows more quickly in the SC sample, $N_{eff}(\omega)$ is nearly equal by $12,000 \text{ cm}^{-1}$ ($\simeq 1.5 \text{ eV}$) for the two materials.²⁸ This effect is similar to the result of Ce doping from $x=.12$ to $x=.2$ in oxygen reduced $\text{Pr}_{2-x}\text{Ce}_x\text{CuO}_{4+\delta}$.¹⁰ The deoxygenation process that takes the AF sample into the superconducting phase is similar to the doping processes in hole doped cuprates. Spectral weight is transferred to lower energies which enhances the metallic response and induces superconductivity.

We now turn to the analysis of the evolution of electron dynamics associated with changes of carrier density from the under doped (AF) region to the optimally doped (SC) sample. A useful optical constant within the context of this discussion is the frequency dependent scattering rate:²⁹

$$1/\tau(\omega) = \frac{\omega_p^2}{4\pi} \text{Re}\left(\frac{1}{\sigma(\omega)}\right). \quad (2)$$

In Fig. 7 we plot $1/\tau(\omega)$ for both the AF sample (left panel) and the SC sample (right panel). Looking first at the right panel we see that above $\omega \sim 650 \text{ cm}^{-1}$ $1/\tau(\omega)$ varies nearly linearly with ω . However, at lower frequencies $1/\tau(\omega)$ drops faster than this linear trend. The low frequency suppression is strongest at 25 K, yet persists even at room temperature. The top of the "shoulder" in $1/\tau(\omega)$ is chosen as the frequency, Θ , characterizing the low energy depression of $1/\tau(\omega)$.

Turning to the AF sample we again see the low frequency suppression of $1/\tau(\omega)$ which is now much more

pronounced. In addition, the magnitude of the scattering rate is nearly twice that of the SC sample. However, the characteristic frequency remains at $\Theta = 650 \text{ cm}^{-1}$ as in the SC sample. The frequency dependence of $1/\tau(\omega)$ also remains nearly linear above Θ ,³⁰ but there is less temperature dependence in this region than found in the SC sample.

Several features of $1/\tau(\omega)$ described above for NCCO are characteristic of the pseudogap state in hole doped cuprates.^{13,29,31,32} Fig. 8 shows typical $1/\tau(\omega)$ spectrum for under and weakly over hole doped Bi2212 .³¹ Examining first the under doped compound in the left panel, the most prominent feature is the depression of $1/\tau(\omega)$ below $\simeq 700 \text{ cm}^{-1}$ in both the normal and superconducting state. This depression is absent at 292 K were the linear high- ω trend continues to the lowest frequencies, yet is clearly well developed at $T > T_c$. This reduction of the scattering rate has been attributed to the opening of a partial gap, or pseudogap, in the density of states. In Bi2212 and other hole doped cuprates the pseudogap has been shown to have the same $d_{x^2-y^2}$ symmetry and similar magnitude as the superconducting gap.³³ Turning to the over doped sample in the right panel we see that the feature in $1/\tau(\omega)$ is now only observed in the superconducting state. The overall magnitude of the scattering is much smaller, and at high frequencies $1/\tau(\omega)$ is temperature dependent. The doping dependent trends of $1/\tau(\omega)$ are consistent with a variety of other measurements:¹³ in the under doped phase a pseudogap opens at a temperature $T^* > T_c$, with an energy scale $\Theta \simeq 2\Delta$, while the pseudogap is absent above T_c in the over doped phase.

Looking back at the NCCO data in Fig. 7 we can see several features that are common to $1/\tau(\omega)$ in the hole doped cuprates. The onset of the depression in $1/\tau(\omega)$ remains at $\Theta = 650 \text{ cm}^{-1}$, independent of doping. The magnitude of $1/\tau(\omega)$ is higher in the under doped samples, and the onset of the depression is much sharper. As doping increases the low energy suppression of $1/\tau(\omega)$ decreases. In addition a strong temperature dependence is observed across the energy range displayed for the more heavily doped samples. There are a few marked differences with the NCCO data. First, $1/\tau(\omega)$ in the superconducting state (not shown) is nearly identical to the 25 K spectrum above 150 cm^{-1} . This is a result of an anomalously small superfluid density, as will be discussed in the next section. The second main difference is that the depression in $1/\tau(\omega)$ is observed at all temperatures, suggesting T^* exceeds 292 K in both the AF and SC samples. This latter result may resolve a long standing discrepancy between the linear temperature dependent resistivity of optimally doped hole cuprates³⁴ and the nearly quadratic temperature dependent resistivity in NCCO. In the pseudogap state ($T < T^*$) $\rho(T)$ decreases faster than linear with decreasing temperature, possibly accounting for the anomalous behavior found in NCCO. In fact recent experiments have found a nearly linear $\rho(T)$ at $T > 292 \text{ K}$ in NCCO.³⁵

The observation of a pseudogap in NCCO ($T_c = 25$

K) with a characteristic temperature $T^* > 300$ K, has significant implications on our theoretical understanding of this phenomenon. In particular, our data suggest that the pseudogap may be distinct from the superconducting gap. Determining the relationship between the pseudogap and superconducting state has become a central problem in the field of high temperature superconductivity.¹⁴ Because many electronic and magnetic properties such as Fig. 8 (left panel) and others³³ evolve smoothly from the pseudogap to superconducting state, the pseudogap is often considered a precursor of the superconducting gap. In addition, the similarities of the energy scales associated with the pseudogap and superconducting states has also been used to support this view. In contrast, in the present experimental work these energy scales are much different. The pseudogap energy scale, Θ , extracted from $1/\tau(\omega)$ is roughly the same as found in the hole doped cuprates (about 5 - 10% less). However, recent photoemission work⁶ on NCCO indicate that the superconducting gap is as small as $2\Delta \simeq 3$ meV, more than an order of magnitude smaller than Θ . These data clearly suggest that in NCCO the pseudogap, as determined from $1/\tau(\omega)$, is not the same as the superconducting gap. Whether this conclusion will hold in other cuprate were the two energy scales are very similar will require further study.

A complimentary interpretation of the pseudogap structure in $1/\tau(\omega)$ may be formulated in terms of charge carriers coupling to a collective mode.^{36,37} At the energy of the mode a new channel of scattering opens for the charge carriers leading to an increase in $1/\tau(\omega)$.³⁸ From an inversion of the $1/\tau(\omega)$ curve the spectrum of the collective mode $W(\omega)$ can be estimated;³⁹

$$W(\omega) = \frac{1}{2\pi} \frac{d^2}{d\omega^2} \left(\omega \frac{1}{\tau(\omega)} \right). \quad (3)$$

The top panel of Fig. 9 shows $1/\tau(\omega)$ at T_c along with the above inversion. The spectra of $W(\omega)$ shows a clear peak at $\omega = 400$ cm^{-1} . Also included in Fig. 9 are a representative collection of $1/\tau(\omega)$ spectra and their corresponding $W(\omega)$ for several different families of electron and hole doped cuprates including single, double, and triple layer materials.^{32,40-42} In all of the materials inversion of $1/\tau(\omega)$ produces similar structure in $W(\omega)$. Recently $W(\omega)$ derived from the $1/\tau(\omega)$ spectra in YBCO has been attributed to antiferromagnetic fluctuations seen as a 41 meV peak in inelastic neutron scattering experiments.³⁹ However, this peak has only been observed in YBCO^{43,44} and Bi2212⁴⁵. Clearly, the remarkable similarities of $1/\tau(\omega)$ and therefore $W(\omega)$ found in different families of cuprates shown in Fig. 9 calls for a uniform description of this feature, rather than ad hoc scenarios for each compound.

While the microscopic origin of the low ω depression in $1/\tau(\omega)$ is unresolved, it is clearly a feature common to all families of cuprate superconductors. This global similarity of the low energy charge dynamics is in agreement

with the suggestion that the pseudogap is a generic feature of the doped Mott-Hubbard insulator.⁴⁶ In addition these results support the idea that the key features of the low energy charge dynamics in high- T_c cuprates are the same for both electron and hole doped materials.

B. Localization in the Cuprates

We now turn to the discussion of the low frequency in-plane conductivity. As pointed out earlier the SC sample shows a peak in $\sigma_1(\omega)$ below 100 cm^{-1} . The peak is unusual because it signals a qualitative departure from a free carrier response. In a wide variety of elemental metals the response of the charge carriers is adequately represented by the Drude model (Eq. 1).⁴⁷ More complex materials in which $\sigma_1(\omega)$ deviates from the Lorentzian form suggested by Eq. 1 the conductivity still remains monotonic as $\omega \rightarrow 0$. The peak in $\sigma_1(\omega)$ at a finite frequency is indicative of charge carrier localization.⁴⁸ In the regime of low dimensionality the electron gas is particularly susceptible to localization effects arising from disorder. Examples can be found in 1-D organic conductors⁴⁹ and 2-D field effect transistors⁵⁰. Localization effects should also not be surprising in the cuprates where the nearly decoupled CuO_2 layers give rise to a quasi 2-D system. In optical studies of controlled induced disorder in ion irradiated $\text{YBa}_2\text{Cu}_3\text{O}_{6.95}$ ⁵¹ and Zn doped $\text{YBa}_2\text{Cu}_4\text{O}_8$ ⁵² a finite frequency peak in $\sigma_1(\omega)$ progressively developed with the introduction of disorder. Other cuprates may show "intrinsic" disorder due to the substitutional process which controls the charge carrier density and induces superconductivity. NCCO may fit in this latter category,⁵³ because the oxygen reduction process leaves a random distribution of oxygen vacancies. Another example of an "intrinsically" disordered system is $\text{Bi}_2\text{Sr}_{2-x}\text{La}_x\text{CuO}_4$ ⁵⁴ where an inhomogeneous distribution of La and Sr doping may give rise to the observed localization effects.⁵⁵

To compare with the NCCO results Fig. 10 shows an example of peaks in $\sigma_1(\omega)$ in hole doped $\text{Bi}_2\text{Sr}_{2-x}\text{La}_x\text{CuO}_4$ for two different levels of La doping.⁵⁴ The main panels show the conductivity in a similar fashion to Fig. 2 and the inset' show the $R(\omega)$ data. Three temperatures are displayed; $T = 10$ K, T_c (28 K for $x=.3$ and 25 K for $x=.4$), and 292 K. The most important feature for this discussion is the obvious maximum seen in $R(\omega)$ spectra near 150 cm^{-1} in both crystals. As discussed earlier the non-monotonic behavior of $R(\omega \rightarrow 0)$ is a clear indication of a finite frequency peak in $\sigma_1(\omega)$. As the main panels show the peaks in $\sigma_1(\omega)$ are similar to that seen in NCCO (Fig. 2). The peak in the $x=.4$ sample is at 90 cm^{-1} and in the $x=.3$ sample it is slightly lower but less well defined. In the superconducting state the peak in both samples softens.

One puzzle with the localization effects observed in the optical conductivity of NCCO and other cuprates is the persistence of "metallic" DC resistivity (positive

$d\rho/dT$). Conventionally the peak in $\sigma_1(\omega)$ is accompanied by an activated DC transport. Moreover, the frequency of the peak in $\sigma_1(\omega)$ agrees well with the activation energy extracted from the resistivity data for 2-D electron gas in Si field-effect transistors.⁵⁰ Nevertheless, a coexistence of the "metallic" resistivity and the peak in $\sigma_1(\omega)$ is a robust result reported for a variety of cuprates. This enigma can be qualitatively understood by considering the complexity of the Fermi surface in the cuprates.⁵⁸ The DC conductivity primarily probes the quasiparticles at the zone diagonal where the d -wave gap has nodes. The optical conductivity is also dominated by the nodal regions. However, electronic states at the zone boundaries $[(\pi, 0)$ or $(0, \pi)]$ are also sampled through the IR measurements as evidenced through the observation of the d -wave pseudogap.^{29,32} According to recent photoemission results, with the systematic addition of impurities, states develop within the gap at $(\pi, 0)$.⁵⁹ This has recently been confirmed through the observation of intra-gap resonance's with scanning tunneling microscopy.⁶⁰ We believe that these resonance's may be connected with the peak observed in $\sigma_1(\omega)$. At the same time the DC transport is effectively shunted by the highly mobile nodal quasiparticles and therefore remains relatively insensitive to the dramatic changes close to the zone boundary.

The effects of disorder are also expected to be prominent in the superconducting state. In a d -wave superconductor disorder leads to pair breaking,⁶¹ and will therefore decrease the total amount of superfluid. Infrared studies have shown that with increasing disorder the superfluid density (ρ_s) is systematically depleted while a concomitant growth of the finite frequency peak in $\sigma_1(\omega)$ is observed.^{51,52} In NCCO we also observe an anomalously small superfluid density. This can be demonstrated from the following sum rule:⁶²

$$\rho_s = \frac{120}{\pi} \int_{0+}^{W_c} [\sigma_1^N(\omega) - \sigma_1^S(\omega)] d\omega \quad (4)$$

where the superscripts N and S refer to the normal and superconducting state. Applying Eq. 4 to the data in Fig. 2 at 7 K and 25 K with the integration cut-off $W_c > 1$ eV we obtain $4 \times 10^7 \text{ cm}^{-2}$. This is only 4%⁶³ of the spectral weight of 10^8 cm^{-2} which corresponds to the penetration depth of $\sim 1500 \text{ \AA}$ reported by microwave and magnetic measurements.^{3,64,65} A similar suppression of ρ_s is found in the data for $\text{Bi}_2\text{Sr}_{2-x}\text{La}_x\text{CuO}_4$ in Fig. 10 and was also reported for other cuprates where a peak in $\sigma_1(\omega)$ is observed.^{51,52,54,41,42}

In contrast to our results, Homes et al.⁸ found a value of $\lambda = 1600 \text{ \AA}$ from the above sum rule analysis, and did not observe a finite frequency peak in $\sigma_1(\omega)$. One possible explanation is that the $T_c = 23$ K crystal was slightly over doped with respect to the crystals measured in this study. In the over doped phase the interlayer coupling of the CuO_2 planes increases and a more 3-D character develops, making samples less susceptible to

localization effects. Doping dependent studies on NCCO and other cuprates showing signs of localization would help clarify this matter.

C. Interlayer Transport

In contrast to the changes in the optical response of the a -axis when varying the oxygen content, there is very little difference between the SC and AF samples along the c -axis (Fig. 4). The matrix element that dominates interlayer transport in cuprates has been shown to have the same symmetry as the d -wave gap: nodes at $(\pi, 0)$ and anti-nodes at (π, π) .⁶⁶ Therefore our polarized infrared measurements can be viewed as an indirect probe of doping dependent changes in the Fermi surface topology. If this interpretation is applied to the results shown in Fig. 4, one can conclude that the oxygen reduction procedure that induces superconductivity has very little effect on the Fermi surface near $(\pi, 0)$. This is also confirmed by the observation of a pseudogap (which is a $(\pi, 0)$ effect³³) in the in-plane scattering rate for both the AF and SC samples. In contrast, Figures 1-3 show that the low energy excitations on other parts of the Fermi surface are dramatically altered. The oxygen reduction process appears to have the largest impact near the zone diagonals. Angle resolved photoemission and other k -dependent probes would be useful in confirming this result.

The most obvious change in the interlayer transport with oxygen doping is the low frequency plasmon that develops due to the presence of superconducting carriers. From the location of this plasmon a value of $\lambda_c = 26 \text{ \mu m}$ is found (Section III-B), in good agreement with Terahertz transmission measurements on thin films of NCCO.⁶⁷ It has been shown^{68,69} that a universal correlation exists between λ_c and $\sigma_1(\omega \rightarrow 0, T_c)$ in the hole doped cuprates. This correlation is given by $\lambda_c^{-2} = \Omega \sigma_1(\omega \rightarrow 0, T_c)$, where Ω is related to the energy scale from which the superfluid is collected. The dark solid line in Fig. 11 represents this correlation for hole doped cuprates.⁶⁹ Other anisotropic superconductors that have conventional normal and superconducting properties also follow this correlation (thin line) but have a smaller constant of proportionality Ω . Organic superconductors, Josephson junctions prepared from elemental metals, transition metal dichalcogenides, and granular films belong to this latter group. Our results for NCCO are shown in the plot as a star. NCCO clearly belongs to the same universality class as the hole doped cuprates. The origin for the different scaling behavior between the cuprates and other anisotropic superconductors is as yet unresolved, but may be related to the incoherent nature of the conductivity discussed below.

In order to understand the impact of the superconducting transition on the interlayer transport it is useful to examine the distinct contributions to $\sigma(\omega)$. In the superconducting state the conductivity can be represented

by two components:

$$\sigma^s(\omega) = \sigma^{pair}(\omega) + \sigma^{reg}(\omega). \quad (5)$$

The first term represents the paired carriers and is given by $\sigma_1^{pair}(\omega) = \rho_s \delta(\omega=0)/8$. The second term corresponds to unpaired carriers below T_c and is plotted in the right panel of Fig. 5. While $\sigma_1^{pair}(\omega)$ is outside of the range of our experiment, the formation of ρ_s which gives rise to this term can be seen in the energy loss function, $\text{Im}(-1/\epsilon)$, plotted in the inset of Fig. 5. In a conducting material the loss function shows a peak at a frequency proportional to the carriers plasma frequency. Looking at the plot of $\text{Im}(-1/\epsilon)$ we see that at $T = T_c$ (thin black line) the loss function is flat and featureless corresponding to an over-damped plasmon. As the temperature is reduced below T_c a sharp resonance develops signaling the formation of ρ_s .

The development of ρ_s must be contrasted with the behavior of $\sigma_1(\omega)$ in Fig. 5. From the sum rule in Eq. 4 we see that as ρ_s increases there should be a corresponding decrease in $\sigma_1(\omega)$ at finite frequencies. What is actually observed is much different. At 19 K, where the peak in the loss function indicates a non-zero superfluid density, $\sigma_1(\omega)$ is larger than the normal state curve at all frequencies shown in Fig. 5. In fact above 50 cm^{-1} the absorption is greater at all temperatures in the superconducting state compared to the normal state curve at 25 K. In order to better elucidate this behavior we rewrite Eq. 4 as $\rho_s = \frac{120}{\pi} \int_{0+}^{W_c} [\sigma_1^N(\omega) - \sigma_1^S(\omega)] d\omega + \Delta K$, where we have split the integral in two⁷⁰:

$$\Delta K = \frac{120}{\pi} \int_{W_c}^{\infty} [\sigma_1^N(\omega) - \sigma_1^S(\omega)] d\omega. \quad (6)$$

ΔK represents the contribution to $\delta(0)$ from the experimentally inaccessible integration region. For the c-axis, above 120 cm^{-1} the electronic component of the conductivity is overwhelmed by the response of the phonons. Therefore the limit of integration is taken as $W_c = 120 \text{ cm}^{-1}$, which corresponds to $\sim 8\Delta$.⁶ While the absolute value of W_c is small, it is worth noting that in all hole doped cuprates that have been studied,^{71,72} $\sigma_1^S \simeq \sigma_1^N$ all ready at 2Δ , and this equality continues throughout the experimentally available range ($\sim 20\Delta$).

The analysis of Eq. 6 reveals the energy scale of the electronic states that make up the superconducting condensate. In order to determine the relative amount of ρ_s originating from $\omega > W_c$ we define the normalized missing spectral weight (NMSW) as $\Delta K(T)/\rho_s(T)$. This ratio gives the fraction of the total δ -function spectral weight drawn from $\omega > W_c = 8\Delta$. The NMSW is plotted as a function of reduced temperature in Fig. 12. This fraction is close to 1 below $.5T_c$, but increases well above 1 as $T \rightarrow T_c$. The inequality $\Delta K(T)/\rho_s(T) > 1$ means that in addition to the growth of ρ_s at $\omega=0$, the finite frequency spectral weight at $\omega < W_c$ increases below T_c . While there has been an effort to understand the NMSW

in other cuprates where $0 < \Delta K/\rho_s < 1$,^{70,73-77} there is currently no theoretical basis in which to understand the inequality $\Delta K/\rho_s > 1$.

In order to clarify the role of the cut-off W_c in the analysis of the energy scales involved in the formation of the superconducting condensate we repeat our analysis with a model BCS system. In conventional superconductors which follow the BCS formalism the formation of ρ_s is always accompanied by a *decrease* in low frequency spectral weight at $T < T_c$, in accord with Eq. 4. The inset of Fig. 12 gives an example of $\sigma_1(\omega)$ for a BCS superconductor in the dirty limit⁷⁸. In the superconducting state of the model $\sigma_1(\omega)$ is zero below 2Δ , then increases sharply and merges with the normal state conductivity. The effect of W_c on Eq. 6 for this model calculation is shown in the main panel. For all values of W_c the NMSW is constant with temperature. The NMSW is always less than 1, regardless of the choice of W_c . For $W_c = 2\Delta$, half of ρ_s is drawn from $\omega > W_c$. However, with $W_c = 8\Delta$, similar to our experimental cutoff, only 7% of ρ_s comes from $\omega > W_c$. This example merely reflects the fact that in the BCS model of superconductivity the electronic states that form the condensate lie near the Fermi energy. In contrast, the differences seen in the NMSW of NCCO indicate that ρ_s is being collected from an extended energy range, by far exceeding the superconducting gap.

In BCS theory, there is only one energy scale involved in superconductivity: the superconducting gap, Δ . However, the data for NCCO suggests that Δ plays little if any role in determining the region from which ρ_s is collected. This indicates that there is an additional energy scale which is greater than 8Δ , in cuprate superconductors.^{70,77}

Studies on the doping dependence of the NMSW in $\text{Ti}_2\text{Ba}_2\text{CuO}_{6+\delta}$ ⁷⁹ and $\text{YBa}_2\text{Cu}_3\text{O}_{6+\delta}$ ⁷² have found this effect to be largest in under doped compounds. The conclusion drawn from these experiments is that when the normal state is incoherent, with low spectral weight, the superfluid is derived from high energies. As a more coherent response develops at low frequencies, the superfluid is formed from this spectral weight near $\omega = 0$. The incoherent conductivity which drives the source of ρ_s to higher energies has been linked to the normal state pseudogap.⁷² For technical reasons we were not able to observe a pseudogap in the c-axis conductivity of NCCO.⁸⁰ However, the extremely small values of $\sigma_1(\omega)$ along with the absence of any obvious Drude peak in the interlayer conductivity is consistent with strongly incoherent transport. The source of the large NMSW shown in Fig. 12 is likely to be tied to the incoherent conductivity as in the hole doped cuprates.

V. CONCLUSIONS

To conclude we find several similarities between NCCO and the hole doped cuprates. The analysis of $1/\tau(\omega)$ in

the SC sample provides strong evidence for a pseudogap in the electron side of the cuprate phase diagram. In addition, the trends seen in the evolution of $1/\tau(\omega)$ from the under doped AF sample to the optimally doped SC sample closely follow the behavior of the hole doped cuprates. In NCCO the pseudogap energy scale Θ is more than an order of magnitude greater than 2Δ . This result implies that, at least in NCCO, the pseudogap and superconducting gap are not the same.

The peak seen in the in-plane conductivity, along with a low value of ρ_s is often observed in disordered hole doped cuprates. Disorder in low dimensional materials, such as the cuprates, often results in charge carrier localization. However, the non-trivial topology of the Fermi surface in the cuprates may lead to a coexistence of localization features in $\sigma_1(\omega)$ with metallic DC transport.

A sum rule analysis of the c-axis conductivity reveals similar trends as is observed in hole doped cuprates. Namely, the spectral weight that is transferred to the delta-function peak at $\omega = 0$ below T_c originates from an energy range in excess of 8Δ . This is fundamentally different from the behavior of conventional superconductors, and indicates a large energy scale is involved in superconductivity in both electron and hole doped cuprates. In addition a comparison of the normal and superconducting properties in NCCO clearly places it in the same universality class as the hole doped cuprates as opposed to other conventional layered superconductors.

This work was supported by the NSF grant DMR-9875980 and the Alfred P. Sloan Foundation. D.N. Basov is a Cottrell Fellow of the Research Corporation.

*Present address: Kohzu Seiki Co., Setagaya 1-8-19, Tokyo, Japan

¹ Y. Tokura, H. Takagi, S. Uchida, Nature **377** 345 (1989); H. Takagi, S. Uchida, Y. Tokura, PRL **62** 1197 (1989)

² The assignment of electrons as the charge carriers is based on the negative value of the Hall coefficient. However, a two band model with both electrons and holes acting as charge carriers has been proposed to account for the less than trivial behavior of the Hall coefficient. Wu Jiang, S.N. Mao, X.X. Xi, X. Jiang, J.L. Peng, T. Venkatesan, C.J. Lobb, R.L. Greene, PRL **73** 1291 (1994); S.I. Woods, A.S. Katz, M.C. de Andrade, J. Herrmann, M.B. Maple, R.C. Dynes, PRB **58** 8800 (1998)

³ D.H. Wu, J. Mao, S.N. Mao, J.L. Peng, X.X. Xi, T. Venkatesan, R.L. Greene, PRL **70** 85 (1993)

⁴ J.D. Kokales, P. Fournier, L.V. Mercaldo, V.V. Talanov, R.L. Greene, S.M. Anlage, PRL **85** 3696 (2000)

⁵ R. Prozorov, R.W. Giannetta, P. Fournier, R.L. Greene, PRL **85** 3700 (2000)

⁶ T. Sato, T. Kamiyama, T. Takahashi, K. Kurahashi, K. Yamada, Science **291** 1517 (2001); N.P. Armitage, D.H. Lu,

D.L. Feng, C. Kim, A. Damascelli, K.M. Shen, F. Ronning, Z.-X. Shen, Y. Onose, Y. Taguchi, Y. Tokura, PRL **86** 1126 (2001)

⁷ C.C. Tsuei, J.R. Kirtley, PRL **85** 182 (2000)

⁸ C.C. Homes, B.P. Clayman, J.L. Peng, R.L. Greene, PRB **56** 5525 (1997)

⁹ Y.J. Uemera G.M. Luke, B.J. Sternlieb, J.H. Brewer, J.F. Carolan, W.N. Hardy, R. Kadono, J.R. Kempton, R.F. Kiefl, S.R. Kretzmann, P. Mulhern, T.M. Rise-man, D.L. Williams, B.X. Yang S.Uchida, H. Takagi, J. Gopalakrishnan, A.W. Sleight, M.A. Subramanian, C.L. Chien, M.Z. Cieplak, G. Xiao, V.Y. Lee, B.W. Statt, C.E. Stronach, W.J. Kossler, X.H. Yu, PRL **62** 2317 (1989)

¹⁰ S.L. Cooper, G.A. Thomas, J. Orenstein, D.H. Rapkine, A.J. Millis, S-W. Cheong, A.S. Cooper, Z. Fisk, PRB **41** 11605 (1990)

¹¹ S. Uchida, T. Ido, H. Tagaki, T. Arima, Y. Tokura, S. Tajima, PRB **43** 7942 (1991)

¹² S. Lupi, P. Calvani, M. Capizzi, P. Maselli, W. Sadowski, E. Walker, PRB **45** 12470 (1992); S. Lupi, M. Capizzi, P. Calvani, B. Ruzicka, P. Maselli, P. Dore, A. Paolone, PRB **57** 1248 (1998); S. Lupi, P. Maselli, M. Capizzi, P. Calvani, P. Giura, P. Roy, PRL **83** 4852 (1999)

¹³ T. Timusk, B. Statt, Rep. Prog. Phys. **62** 61 (1999)

¹⁴ For a perspective see M Buchanan, Nature **409** 8 (2001)

¹⁵ A gap-like feature in $\sigma_1(\omega)$ has been observed in NCCO by Onose and coworkers at .3 eV.¹⁶ Similar structure has not been detected in other cuprates. The typical energy scale of the pseudogap in the hole doped cuprates is ~ 90 meV.

¹⁶ Y. Onose, T. Taguchi, T. Ishikawa, S. Shinomori, K. Ishizaka, Y. Tokura, PRL **82** 5120 (1999)

¹⁷ B. Stadlober, G. Krug, R. Nemetschek, R. Hackl, J.L. Cobb, J.T. Market PRL **74** 4911 (1995)

¹⁸ K. Kurahashi, PhD Thesis, Tohokura University (1999)

¹⁹ M. Matsuda, Y. Endoh, K. Yamada, H. Kojima, I. Tanaka, R.J. Birgeneau, M.A. Kastner, G. Shirane, PRB **45** 12548 (1992)

²⁰ S. Jandl, P. Dufour, T. Strach, T. Ruf, M. Cardona, V. Nekvasil, C. Chen, B.M. Wanklyn, PRB **52** 15558 (1995)

²¹ C.C. Homes, M. Reedyk, D.A. Cradles, T. Timusk, Applied Optics **32** 2976 (1993)

²² T. Arima, Y. Tokura, S. Uchida, PRB **48** 6597 (1993)

²³ Y. Hidaka, M. Suzuki, Nature **338** 635 (1989)

²⁴ M.C. de Andrade, Y. Dalichaouch, M.B. Maple, PRB **48** 16737 (1993)

²⁵ W. Jiang, S.N. Mao, X.X. Xi, X. Jiang, J.L. Peng, T. Venkatesan, C.J. Lobb, R.L. Greene, PRL **73** 1291 (1994)

²⁶ H. Takagi, S. Uchida, Y. Tokura, PRL **62** 1197 (1989)

²⁷ A.J. Schultz, J.D. Jorgensen, J.L. Peng, R.L. Greene, PRB **53** 5157 (1996)

²⁸ The different carrier densities for the two samples produced by the oxygen reducing procedure would dictate that N_{eff} is crossing at $14,000 \text{ cm}^{-1}$ rather than saturating to a constant value.

²⁹ For an overview see: A.V. Puchkov, D.N. Basov, T. Timusk, Journal of Physics and Condensed Matter **8** 10049 (1996)

³⁰ For $\omega > 700 \text{ cm}^{-1}$ $1/\tau(\omega)$ is not shown for the AF sample

- at 25 K and 80 K, as another channel of absorption opens and the scattering rate description is not appropriate at these energies.
- ³¹ A.V. Puchkov, P. Fournier, D.N. Basov, T. Timusk, A. Kapitulnik, N.N. Kolesnikov, PRL **77** 3212 (1996)
- ³² D.N. Basov, R. Liang, B. Dabrowski, D.A. Bonn, W.N. Hardy, T. Timusk, PRL **77** 4090 (1996)
- ³³ A.G. Loeser, Z.-X. Shen, D.S. Dessau, D.S. Marshall, C.H. Park, P. Fournier, A. Kapitulnik, Science **273** 325 (1996); H. Ding, T. Yokoya, J.C. Campuzano, T. Takahashi, M. Randeria, M.R. Norman, T. Mochiku, K. Hadowaki, J. Giapintzakis, Nature, **382** 51 (1996)
- ³⁴ H. Takagi, B. Batlogg, H.L. Kao, J. Kwo, R.J. Cava, J.J. Krajewski, W.F. Peck, PRL **69** 2975 (1992)
- ³⁵ R. Greene *private communication*
- ³⁶ Z.X. Shen, J.R. Schrieffer, PRL **78** 1771 (1997); M.R. Norman, H. Ding, PRB **57** 11089 (1998); D. Munzar, C. Bernhard, M. Cardona, Physica C **317-318** 547 (1999); R. Haslinger, A.V. Cubukov, Ar. Abanov, PRB **63** 20503 (2000)
- ³⁷ The threshold structure in the spectra of $1/\tau(\omega)$ corresponds to a "kink" in the dispersion dependence probed through ARPES measurements. Recently Z.X. Shen *et al.* reported an observation of this feature in several different families of cuprates [*cond-mat/0102244*].
- ³⁸ P.B. Allen, PRB **3** 305 (1971)
- ³⁹ J.P. Carbotte, E. Schachinger, D.N. Basov, Nature **401** 354 (1999)
- ⁴⁰ A.V. Puchkov, T. Timusk, S. Doyle, A.M. Hermann, PRB **51** 3312 (1995)
- ⁴¹ T. Startseva, T. Timusk, A.V. Puchkov, D.N. Basov, H.A. Mook, M. Okuya, T. Kimura, K. Kishio, PRB **59** 7184 (1999)
- ⁴² J.J. McGuire, M. Windt, T. Startseva, T. Timusk, D. Colson, V. Viallet-Guillen, *cond-mat/9912338*
- ⁴³ H.F. Fong, B. Keimer, D. Reznik, D.L. Milius, I.A. Aksay, PRB **54** 6708 (1996)
- ⁴⁴ P. Dai, M. Yethiraj, H.A. Mook, T.B. Lindemer, F. Dogan, PRL **77** 5425 (1996)
- ⁴⁵ H.F. Fong, P. Bourges, Y. Sidis, L.P. Regnault, A. Ivanov, G.D. Gu, N. Koshizuka, B. Keimer, Nature **398** 588 (1999)
- ⁴⁶ C. Huscroft, M. Jarrell, Th. Maier, S. Moukouri, A.N. Tahvildarzadeh, PRL **86** 139 (2001)
- ⁴⁷ M.A. Ordal, L.L. Long, R.J. Bell, S.E. Bell, R.R. Bell, R.W. Alexander, C.A. Ward, Applied Optics, **22** 1099 (1983)
- ⁴⁸ W. Gotze, P. Wolfe, PRB **6** 1226 (1972)
- ⁴⁹ R.S. Kohlman and A.J. Epstein in *Handbook of conducting polymers* Ed. T.A. Skotheim, R.L. Elsenbaumer, J.R. Reynolds (M. Decker, New York 1998) p.85
- ⁵⁰ S.J. Allen, D.C. Tsui, F. DeRosa, PRL **35** 1359 (1975)
- ⁵¹ D.N. Basov, A.V. Puchkov, R.A. Hughes, T. Strach, J. Preston, T. Timusk, D.A. Bonn, R. Liang, W.N. Hardy, PRB **49** 12165 (1994)
- ⁵² D.N. Basov, B. Dabrowski, T. Timusk, PRL **81** 2132 (1998)
- ⁵³ An alternative explanation for these results is that the systems are macroscopically inhomogeneous, consisting of metallic and insulating regions. The mixed phase system can give rise to a peak in $\sigma_1(\omega)$.⁴⁹
- ⁵⁴ C. Weber, D.N. Basov, R. Yoshazki, *unpublished*
- ⁵⁵ Other cuprates that have shown low frequency peaks in $\sigma_1(\omega)$ include $\text{Tl}_2\text{Ba}_2\text{CuO}_{6+\delta}$ ⁴⁰, under doped $\text{La}_{1.86}\text{Sr}_{1.14}\text{CuO}_4$ ⁴¹, the three layered compound $\text{HgBa}_2\text{Ca}_2\text{Cu}_3\text{O}_{8+\delta}$ ⁴², the single layer $\text{Bi}_2\text{Sr}_2\text{CuO}_6$ ⁵⁶, and the non-superconducting quasi 1-D compound $\text{Sr}_{1-x}\text{Ca}_x\text{Cu}_{24}\text{O}_{41}$ ⁵⁷.
- ⁵⁶ S. Lupi, P. Calvani, M. Capizzi, P. Roy, *cond-mat/0001244*
- ⁵⁷ T. Osafune, N. Motoyama, H. Eisaki, S. Uchida, S. Tajima, PRL **82** 1313 (1999)
- ⁵⁸ Z.-X. Shen, W.E. Spicer, D.M. King, D.S. Dessau, B.O. Wells, Science **267** 343 (1995)
- ⁵⁹ I. Vobornik, H. Berger, D. Pavuna, M. Onellion, G. Margaritondo, F. Rullier-Albenque, L. Forro, M. Grioni, PRL **82** 3128 (1999)
- ⁶⁰ S.H. Pan, E.W. Hudson, K.M. Lang, H. Eisaki, S. Uchida, J.C. Davis, Nature **403** 746 (2000)
- ⁶¹ R.J. Radtke, K. Levin, H.B. Schuttler, M.R. Norman, PRB **48** 653 (1993); M. Franz, C. Kallin, A.J. Berlinsky, PRB **54** 6897 (1996)
- ⁶² M. Tinkham, R.A. Ferrell, PRL **2** 331 (1959)
- ⁶³ It should be noted that there are substantial errors in the absolute value of $\sigma_1(\omega)$ near the peak. The absorption is proportional to $1-R(\omega)$, which from examination of Fig. 1 is very small at low temperatures. Therefore our error in the absolute values of $R(\omega)$ of $\pm 1\%$ causes a large uncertainty in $\sigma_1(\omega)$. For example, a reduction of the 25 K reflectance by 1% cuts the magnitude of the peak in $\sigma_1(\omega)$ by 50% . However, the relative error which is an order of magnitude smaller is the relevant error when applying Eq. 4. Taking this error into consideration Eq. 4 still accounts for less than 5% of the spectral weight corresponding to published values of the penetration depth.
- ⁶⁴ F. Gollnik, M. Naito, PRB **58** 11734 (1998)
- ⁶⁵ A.A. Nugroho, I.M. Sutjahja, A. Rusydi, M.O.Tjia, A.A. Menovsky, F.R. de Boer, J.J.M. Franse, PRB **60** 15384 (1999)
- ⁶⁶ S. Chakravarty, A. Sudbo, P.W. Anderson, S. Strong, Science **261** 337 (1993); O.K. Andersen, A.I. Liechtenstein, O. Jepsen, F. Paulsen, J. Phys. Chem. Solids **56** 1573 (1995); T. Xiang, C. Panagopoulos, J.R. Cooper, Int. J. of Mod. Phys. B **12** 1007 (1998)
- ⁶⁷ A. Pimenov, A.V. Pronin, A. Loidl, U. Michelucci, A.P. Kampf, S.I. Krasnosvobodtsev, V.S. Nozdrin, D. Rainer, *cond-mat/0005515*
- ⁶⁸ D.N. Basov, T. Timusk, B. Dabrowski, J.D. Jorgensen, PRB **50** 3511 (1994)
- ⁶⁹ S.V. Dordevic, E.J. Singley, D.N. Basov, J.H. Kim, M.B. Maple, E. Bucher, *cond-mat/0102455*
- ⁷⁰ J.E. Hirsch, Physica C **199** 305 (1992)
- ⁷¹ D.N. Basov, S.I. Woods, A.S. Katz, E.J. Singley, R.C. Dynes, M. Xu, D.G. Hinks, C.C. Homes, M. Strongin, Science **283** 49 (1999)
- ⁷² D.N. Basov, C.C. Homes, M. Strongin, E.J. Singley, T. Timusk, G. Blumberg, D. van der Marel, *to be published in PRB*
- ⁷³ P.W. Anderson, *The Theory of Superconductivity in the High- T_c Cuprates*, (Princeton University Press, Princeton, 1998); P.W. Anderson, Science **279** 1196 (1998)
- ⁷⁴ S. Chakravarty, Eur. Phys. J. **B5** 337 (1998); S. Chakravarty, H.-Y. Kee, E. Abrahams, PRL **82** 2366

(1999)

⁷⁵ L.B. Ioffe, A.J. Millis, *Science* **285** 1241 (1999)

⁷⁶ W. Kim, J.P. Carbotte, *PRB* **62** 592 (2000)

⁷⁷ M. Imada, S. Onoda, *cond-mat/0008050*

⁷⁸ The parameters used in this calculation are $(1/\tau)/(2\Delta) = 10$, and $T = 0$. W. Zimmermann, E.H. Brandt, M. Bauer, E. Seider, L. Genzel, *Physica C* **183** 99 (1991)

⁷⁹ A.S. Katz, S.I. Woods, E.J. Singley, T.W. Li, M. Xu, D.G. Hinks, R.C. Dynes, D.N. Basov, *PRB* **61** 5930 (2000)

⁸⁰ The observation of a pseudogap requires the analysis of the frequency dependence of $\sigma_1(\omega)$ throughout the FIR. Over most of this range the electronic contribution to $\sigma_1(\omega)$ is overwhelmed by the phonon response, therefore completely masking any changes in $\sigma_1(\omega)$ from the electronic channel.

FIG. 1. Panel A: a-axis far-infrared reflectance of the SC sample at $T = 292, 225, 150, 80, 25$, and 7 K. As the temperature drops a well defined maximum develops at 150 cm^{-1} . The temperature dependence below T_c is confined to $\omega < 100 \text{ cm}^{-1}$. Panel B: a-axis reflectance of the AF sample at the above temperatures. Notice that the y-axis covers a broader range than in panel A. The overall reflectance is lower than that of the SC sample and additional phonon modes are visible. An anomalous structure between 250 cm^{-1} and 450 cm^{-1} is visible at 292 K and grows in strength as the temperature is reduced. Panel C: high frequency reflectance of the SC and AF sample at 292 K and 25 K. The screened plasma frequency (minimum in $R(\omega)$) is the same in both samples. While the 25 K and 292 K spectrum merge smoothly in the SC sample, the 25 K curve in the AF sample crosses below 292 K at $1,000 \text{ cm}^{-1}$ and remains suppressed up to $4,000 \text{ cm}^{-1}$.

FIG. 2. Far-infrared conductivity for the a-axis of the SC sample. At all temperatures there is a finite frequency peak in $\sigma_1(\omega)$. The peak grows in intensity and softens as the temperature is lowered to T_c . Below T_c the peaks intensity is slightly reduced as it further softens. The inset shows $\sigma_1(\omega)$ at 25 K and 292 K up to $4,000 \text{ cm}^{-1}$ where the y-axis has been reduced by nearly an order of magnitude. The peak is clearly visible even at 292 K. The inset shows the canonical pseudogap behavior of $\sigma_1(\omega)$ as seen in the under doped hole cuprates. As the temperature decreases the low frequency peak narrows below a characteristic frequency ($\simeq 650 \text{ cm}^{-1}$).

FIG. 3. A-axis conductivity of the AF sample at 25 K and 292 K. While $\sigma_1(\omega)$ is flat and featureless at 292 K, a broad resonance develops at 25 K. In addition the 25 K spectrum shows a minimum near 400 cm^{-1} similar to the SC sample. The inset shows a second channel of absorption at $\omega \simeq 2,200 \text{ cm}^{-1}$ that develops at low temperatures.

FIG. 4. (Right Panel) c-axis reflectance at 25 K of both the SC (solid lines) and AF sample (dashed-dotted line). Above 100 cm^{-1} the spectra of both samples are nearly identical. Three strong phonons are observed in the far-infrared. The left panel shows the sub-Terahertz reflectance at 25 K and lower temperatures. A slight upturn is seen in the normal state spectra as $\omega \rightarrow 0$ indicating a finite electronic contribution to the conductivity. As the sample becomes superconducting the characteristic plasma edge develops due to the screening of the superconducting carriers. (Temperatures shown: $T = 25, 21, 19, 17, 15, 12$, and 7 K)

FIG. 5. Left Panel: low frequency $R(\omega)$ at 7 K and 25 K plotted on a linear scale. The straight dashed line corresponds to $R(\omega)$ calculated with only the contribution of $\epsilon = 17$. From the location of the minimum in $R(\omega)$ and this value of ϵ we find $\lambda_c = 26 \text{ }\mu\text{m}$ as described in the text. Additionally using ϵ and Eq. 1 we fit (dashed line) $R(\omega)$ at 25 K with $\sigma(\omega = 0)$ as the free variable and obtain a best fit with $\sigma(\omega = 0) = 1.5 \text{ }\Omega^{-1}\text{cm}^{-1}$. Right Panel: electronic contribution to $\sigma_1(\omega)$ in the SC sample below the first phonon. Notice the non-trivial temperature and frequency dependence above and below T_c . The inset shows the peak in the loss function due to the development of the superconducting condensate.

FIG. 6. The a-axis differential conductivity, $\sigma_1^{SC}(\omega) - \sigma_1^{AF}(\omega)$ plotted throughout the infrared. The oxygen reducing procedure leads to spectral weight transfer from the mid-infrared to lower energies. The inset shows that the total spectral weight below $\simeq 14,000 \text{ cm}^{-1}$.

FIG. 7. The in-plane scattering rate (Eq. 2) for the SC (right panel) and AF (left panel) samples. Above 650 cm^{-1} in the SC sample the frequency dependence is linear. At $\omega < \Theta 1/\tau(\omega)$ is suppressed faster than a linear extrapolation of the high frequency data. This suppression can be seen at all temperatures, but is most pronounced at T_c . In the superconducting state (not shown) the spectrum is nearly the same as at $T = T_c$. The AF sample shows a similar, but sharper threshold (arrow) also at 650 cm^{-1} . These spectra should be compared to the $1/\tau(\omega)$ data for hole doped materials in Fig. 8

FIG. 8. The in-plane scattering rate is plotted at 292 K, T_c , and 10 K for under doped Bi2212 (left panel) and slightly over doped Bi/Pb2212 (right panel)³¹. In the under doped compound a gap in $1/\tau(\omega)$ (marked by arrows) opens well above T_c , while in the over doped compound the gap only opens in the superconducting state. Above the gap $1/\tau(\omega)$ is independent of temperature for the under doped system, while it is temperature dependent at all frequencies in the over doped phase.

FIG. 9. Left Panel: $1/\tau(\omega)$ at $T \simeq 10$ K for several different families of high- T_c cuprates.^{32,40-42} All the spectra share a similar low- ω depression with a nearly linear frequency dependence at higher energies. Right Panel: $W(\omega)$ derived from $1/\tau(\omega)$ using Eq. 3. Again, the spectra of $W(\omega)$ all have similar form.

FIG. 10. Main Panels: $\sigma_1(\omega)$ within the CuO_2 plane for $\text{Bi}_{2-x}\text{La}_x\text{Sr}_2\text{CuO}_4$ with $x = .3$ (top panel) and $x = .4$ (bottom panel).⁵⁴ A finite frequency peak can be seen below 100 cm^{-1} in both samples for all temperatures (300 K, T_c , and 10 K shown). The inset show the reflectance data where clear maximum can be seen near 150 cm^{-1} for both dopings.

FIG. 11. Universal plot showing the correlation between $\sigma_{DC}(T=T_c)$ and λ_c^{-2} in layered superconductors.^{68,69} The bottom line corresponds to the hole doped cuprates. The top line includes 2D organic superconductors, transition metal dichalcogenides, granular metal films, and Josephson junctions prepared from elemental metals. Our measurements indicate that NCCO (star in plot) belongs to the same universality class as the hole doped cuprates.

FIG. 12. The normalized missing spectral weight (defined in text), $\Delta K(T)/\rho_s(T)$, show the fraction of the superfluid density collected from $\omega > 8\Delta$ as a function of reduced temperature. The inset shows a calculation of $\sigma_1(\omega)$ above and below T_c for a BCS superconductor in the dirty limit. The lines at the bottom of the main panel shows how $\Delta K(T)/\rho_s(T)$ in this model system depends on the integration limit (W_c) in Eq. 6. Notice that with $W_c = 8\Delta$ only 7% of ρ_s is drawn from higher energies.

Fig. 1

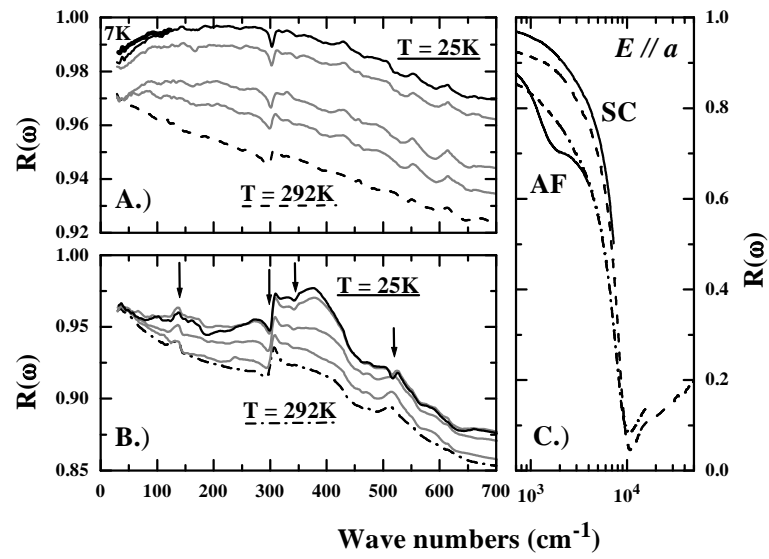


Fig. 2

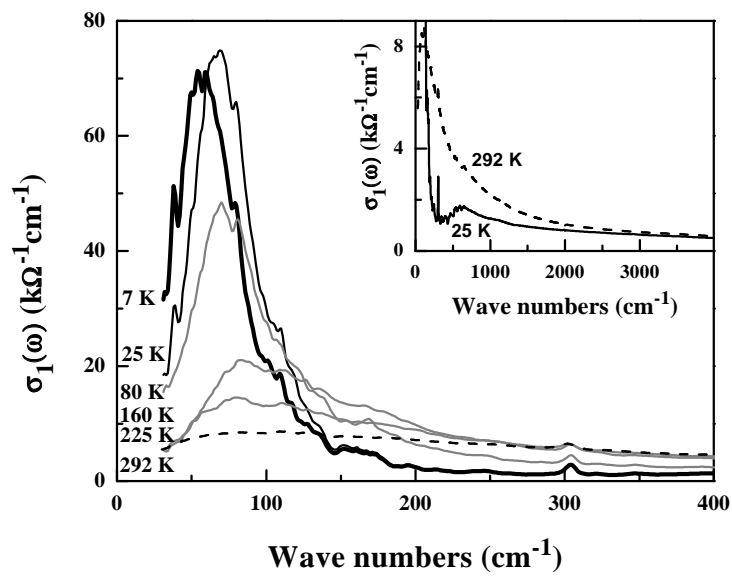


Fig. 3

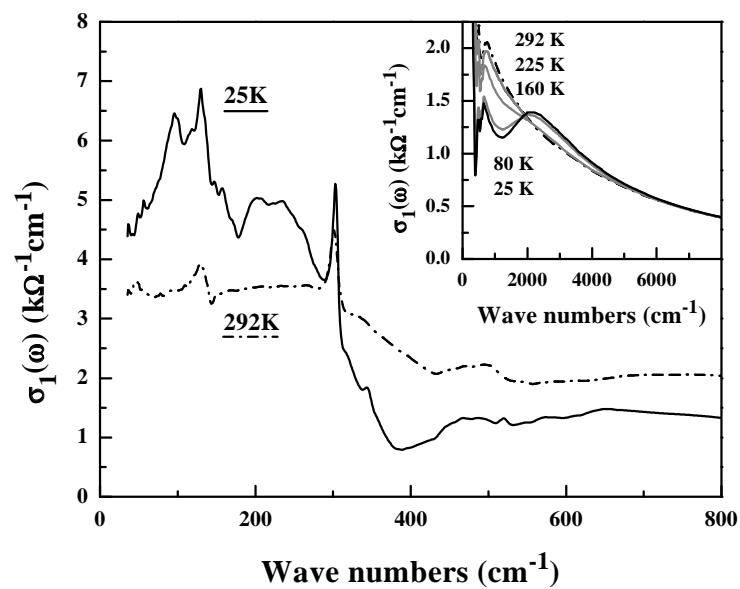


Fig. 4

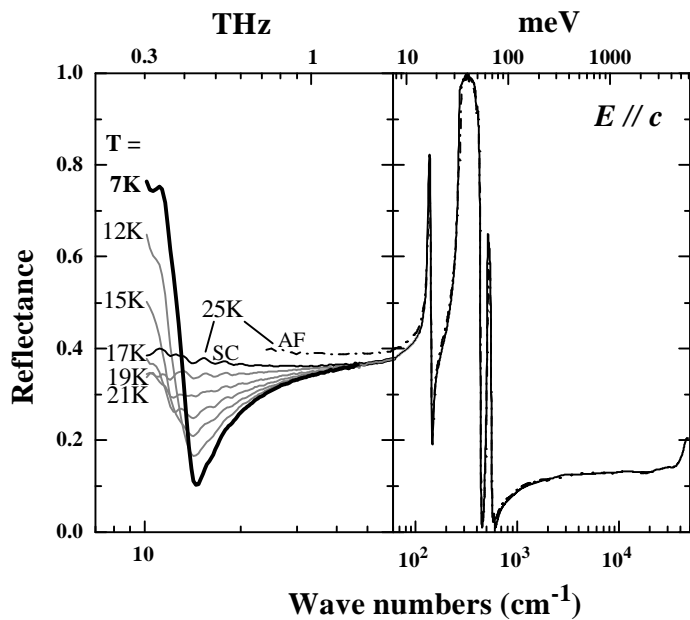


Fig. 5

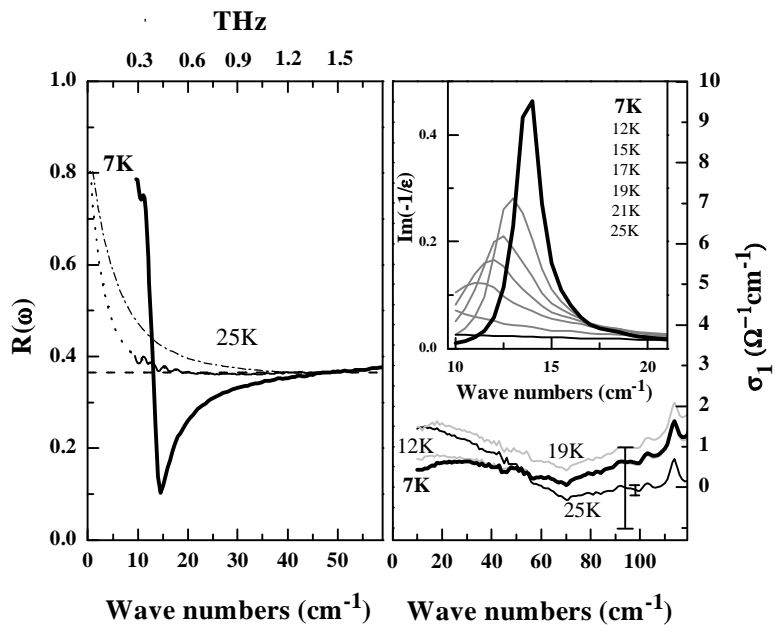


Fig. 6

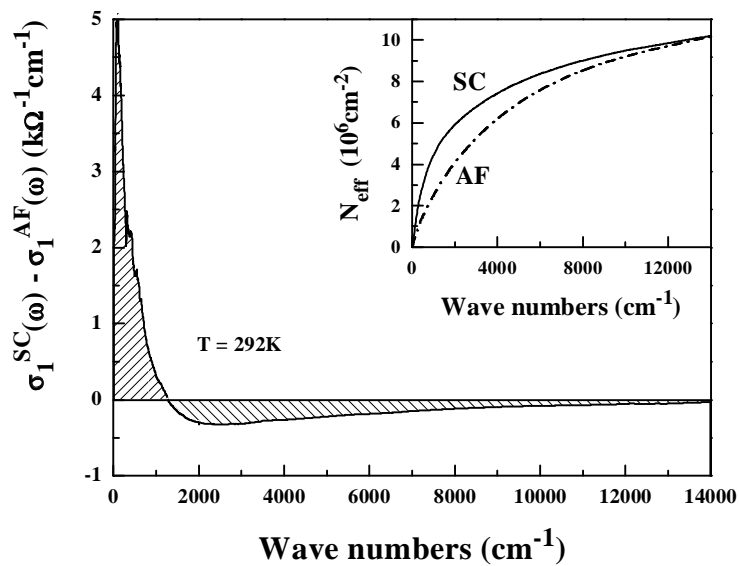


Fig. 7

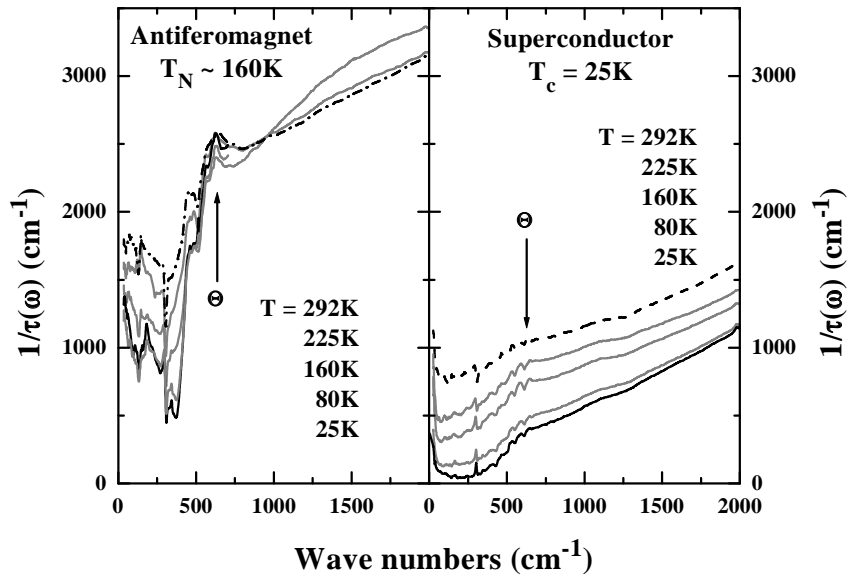


Fig. 8

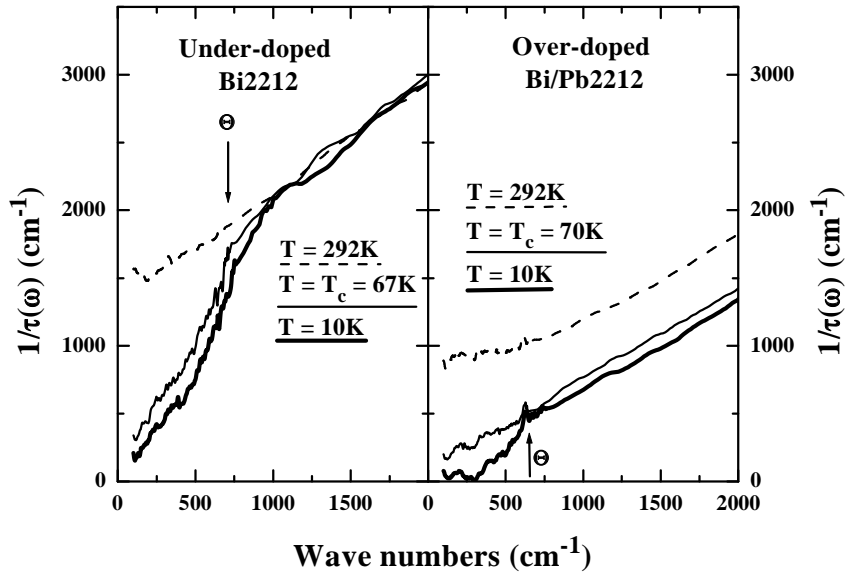


Fig. 9

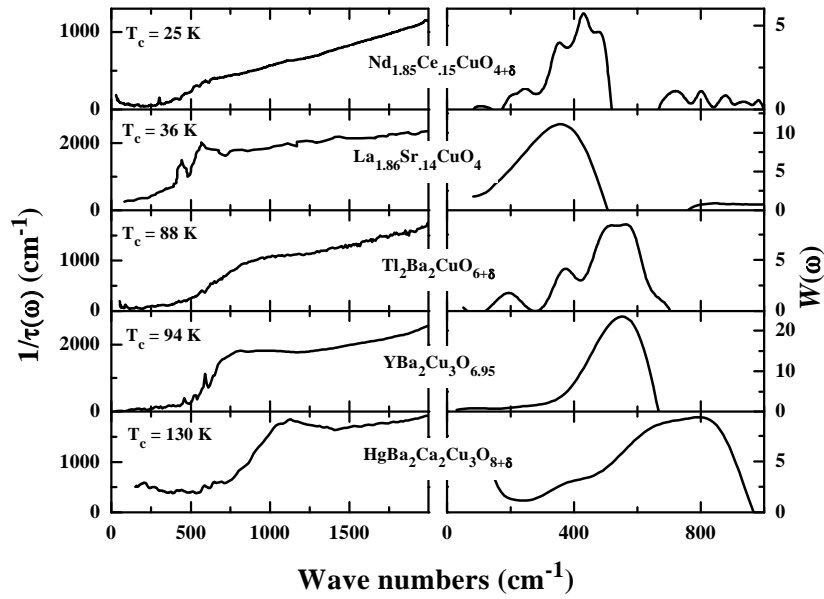


Fig. 10

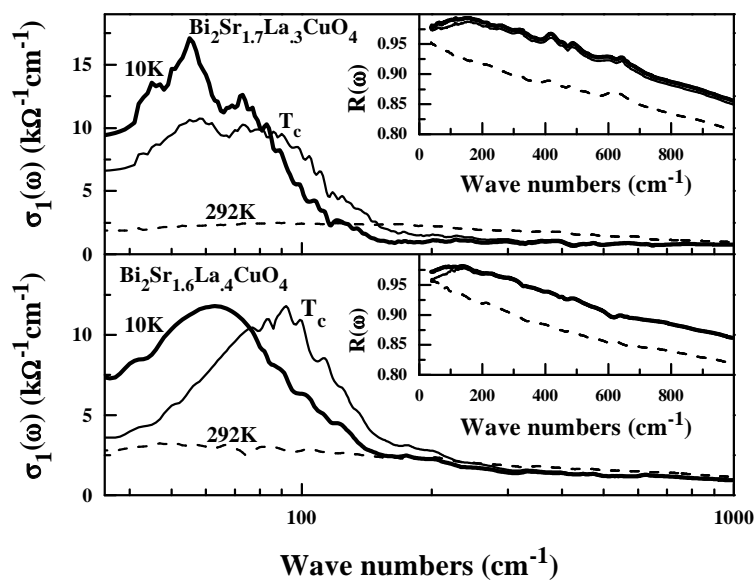


Fig. 11

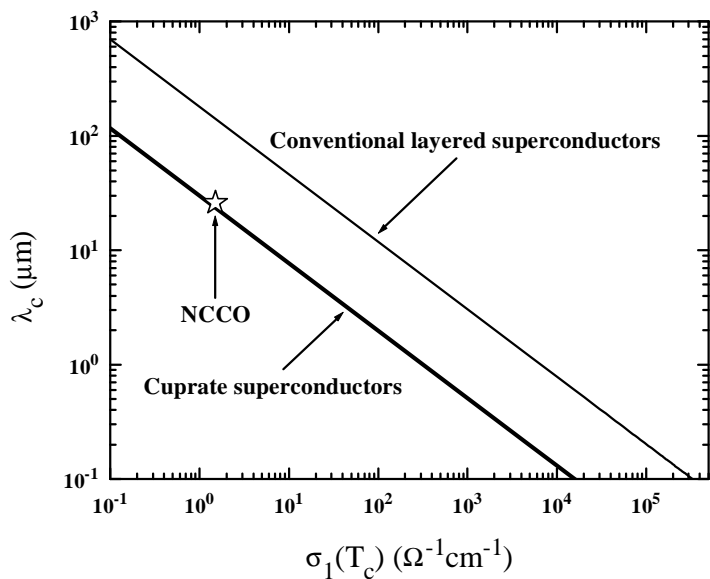


Fig. 12

